Experimental Mechanics (2008) 48:91–106
DOI 10.1007/s11340-007-9076-2

Effect of Pressure on Fluid Damping in MEMS Torsional Resonators with Flow Ranging from Continuum to Molecular Regime

A.K. Pandey · R. Pratap · F.S. Chau

Received: 18 January 2007 / Accepted: 24 July 2007 / Published online: 1 September 2007

Abstract High quality factor of dynamic structures at micro and nano scale is exploited in various applications of micro electro-mechanical systems (MEMS) and nano electro-mechanical system. The quality factor of such devices can be very high in vacuum. However, when vacuum is not desirable or not possible, the tiny structures must vibrate in air or some other gas at pressure levels that may vary from atmospheric to low vacuum. The interaction of the surrounding fluid with the vibrating structure leads to dissipation, thus bringing down the quality factor. Depending on the ambient fluid pressure or the gap between the vibrating and the fixed structure, the fluid motion can range from continuum flow to molecular flow giving a wide range of dissipation. The relevant fluid flow characteristics are determined by the Knudsen number which is the ratio of the mean free path of the gas molecule to the characteristic flow length of the device. This number is very small for continuum flow and reasonably big for molecular flow. In this paper, we study the effect of fluid pressure on the quality factor by carrying out experiments on a MEMS device that consists of a double gimbaled torsional resonator. Such devices are commonly used in optical cross-connects and switches. We only vary fluid pressure to make the Knudsen number go through the entire range of continuum flow, slip flow, transition flow, and molecular flow. We experimentally determine the quality factor of the torsional resonator at different air pressures ranging from 760 Torr to 0.001 Torr. The variation of this pressure over six orders of magnitude ensures required rarefaction to range over all flow conditions. Finally, we get the variation of quality factor with pressure. The result indicates that the quality factor, Q, follows a power law, $Q \propto P^{-r}$, with different values of the exponent r in different flow regimes. In the second part of the paper, we propose the use of effective viscosity for considering velocity slip conditions in solving Navier–Stokes equation numerically. This concept is validated with analytical results for a simple case and then compared with the experimental results presented in this paper. The study shows that the effective viscosity concept can be used effectively even for the molecular regime if the air-gap to length ratio is sufficiently small ($h_0/L < 0.01$). As this ratio increases, the range of validity decreases.

Keywords MEMS · Torsion motion · Squeeze-film damping · Experimental result · Quality factor · Microfluidics

A.K. Pandey (✉) · R. Pratap
CranesSci MEMS Lab, Department of Mechanical Engineering, Indian Institute of Science, Bangalore-560012, India
e-mail: ashok@mecheng.iisc.ernet.in

F.S. Chau
Microsystems Technology Initiative, Department of Mechanical Engineering, National University of Singapore, 10 Kent Ridge Crescent, Singapore 119260, Singapore

Introduction

With the rapid progress of micro and nano fabrication processes in the recent years it is now possible to fabricate miniaturized devices whose size varies from micro to nano scales. Now, the focus is on creating high performance devices which are sensitive and have high quality factor [1–4]. Since the performance of the

dynamic devices depends largely on the damping present in the system, the estimation and means of reducing damping are required. For micro devices which operate at ambient pressure, fluid damping [5–7] is the most dominant damping mechanism. Fluid damping may be due to the air flow around a structure vibrating in isolation or due to squeezing of air in the gap between an oscillating structure and the fixed substrate [8–10]. In this paper, we study the effect of fluid damping in micro electro-mechanical systems (MEMS) torsional resonators which are commonly used as charge detectors, radio-frequency filters, optical cross-connects, switches [11, 12], etc.

Since the fluid flow through a micro or nano channel may not be in the continuum regime either because of their small characteristic dimension or low operating pressure, the rarified gas dynamics is used to model the flow under these conditions [13–15]. A brief theory of rarified gases [16] is discussed in the next section. The rarefaction in gases is mainly characterized by the Knudsen number, Kn, which is the ratio of the mean free path of the air molecules (which depends on the surrounding pressure and temperature) to the characteristics flow length of the channel (which depends on the air-gap thickness of the microchannels) [17]. Based on the different values of Kn, the flow through these channels falls into one of the four flow regimes, viz., continuum regime, slip regime, transition regime, and molecular regime [18]. For continuum regime, $\mathrm{Kn} \to 0$, and for molecular regime, $\mathrm{Kn} \to \infty$. Since rarefaction reduces the viscous effect of the fluid, the fluid damping varies from the highest value in the continuum regime to the lowest value in the molecular regime. Therefore, to increase the device performance, Kn can be increased either by increasing the mean free path of the gas molecules (which is obtained by evacuating the surrounding pressure of the devices to an appropriate pressure) or by reducing the characteristics flow length (which is obtained by reducing the air-gap thickness from micro to nanometer scale) [19]. Since varying the Kn value by taking different flow lengths requires large number of geometrically different test devices, and hence considerable cost in fabrication, we carry out dynamic response study of a microdevice by varying the surrounding pressure. Since the flow conditions obtained by varying the surrounding pressure or the characteristic flow length are equivalent only under certain conditions, we also discuss the relevant similarity laws for the microflows in the next section.

To model the squeeze-film flow in the air-gap between the moving structure and the fixed substrate of the torsional resonator, the conventional Reynolds equation is used [9, 10]. While the Reynolds equation is valid under the assumption of small air-gap thickness to the lateral dimensions, the Navier–Stokes equation can be used to model the flow if the gap is comparable to the lateral dimensions [20]. However, both these equations are valid only in the continuum flow regime. To model the rarefaction effect, either the Boltzmann equation is solved using direct simulation Monte Carlo (DSMC) method [21, 22] or the Navier–Stokes equations are solved with slip boundary conditions [16, 23, 24]. The validity of Navier–Stokes equation, however, is restricted again by the degree of rarefaction, which is briefly discussed in the next section. In this paper, we model the fluid damping using the Navier–Stokes equation with no-slip condition for the flow in the continuum regime and with the higher order slip boundary condition [9, 25] for the flow in the slip, the transition and the molecular regime. Then, we discuss the validity of the numerical results in different flow regimes. In short, we first present a brief theory of the rarified gases and the validity of different governing equations under different flow regimes.

Next, we study the effect of surrounding pressure on the quality factor by carrying out experiments on a MEMS device that consists of a double gimballed torsional resonator as shown in Fig. 1. Although, we only vary pressure to make the Knudsen number go through the entire flow regimes, the same can be obtained by reducing the characteristic flow lengths in a device from micrometer to nanometer under certain conditions. Thus the result presented will hold good for micro-scale to nano-scale devices for damping due to surrounding fluid flow. We obtain an approximate power law (based on the experimental results) governing the variation of the quality factor, Q, with the surrounding pressure, P, for different flow regimes. Next, we numerically model the 3D fluid flow behavior to find the quality factor of

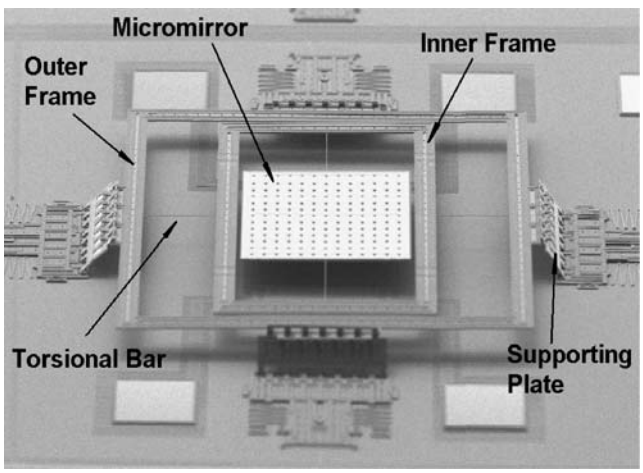

Fig. 1 A picture of double-gimballed MEMS torsion mirror

the device. Since the air-gap thickness of the device (shown in Fig. 1) is comparable to the lateral dimensions, we numerically solve 3D Navier–Stokes equation with slip boundary conditions using ANSYS. Here, the effects of slip boundary condition are included by considering the effective viscosity under different flow regimes. Since, it is an unusual, but a useful, approach to model the rarefaction effect numerically, we first validate this approach by comparing the numerical results with the analytical results for a simple domain and then compare it with the experimental results for the double-gimballed torsional resonator. Finally, we discuss the different source of errors in the experimental and the numerical results.

Brief Theory of Rarified Gases

Under normal conditions, the continuum model is used to model gas flow [8]. In practice, the characteristic length scale of flow under normal conditions has a minimum size of about 1 cm, and a change of 10^{-3} cm would be very small [19]. Subsequently, the change in volume 10^{-9} cm^3 would give the measurement of the local properties of the gas. Since the number density of the gas molecules under standard conditions is 2.69×10^{19} cm^{-3}, the number of molecules in a volume 10^{-9} cm^3 would be 3×10^{10} molecules. This number is sufficiently large to ensure that the average property of the gas is not influenced by the number of molecules in the volume. But under the condition of extremely low density (or when the size of the body is extremely small), discrete particle effects such as velocity slip and temperature jump at the boundaries become significant, and then we have to adopt discrete model, i.e., the method of rarified gas dynamics which considers such effects [24]. This happens when the characteristics flow length becomes so small that it becomes comparable to the molecular mean free path of the gas. The gas flow under this condition is called rarified gas flow [16, 18, 24]. To characterize the degree of rarafaction, the Knudsen number is used which is the ratio of the molecular mean free path λ and the characteristic length of the flow h, and is given by [16]

$$\mathrm{Kn} = \frac{\lambda}{h}. \tag{1}$$

Generally, when $\mathrm{Kn} > 0.1$, the Navier–Stokes equation and the continuum flow model is no longer valid. For $\mathrm{Kn} < 0.1$ but larger than 0.01, some discrete effects such as the velocity slip effect and temperature jump (this effect is negligible in MEMS structures as silicon has sufficiently high thermal conductivity) appear. To discuss the physics of rarefaction effects, we define and discuss the relevant molecular quantities below:

- *Number density of molecules (n)*: The number of molecules in one mole of gas is a constant, known as the **Avogadro's number** which is 6.02252×10^{23}/mole, and the volume occupied by a mole of a gas at a given temperature and pressure is constant irrespective of the composition of the gas. Based on the perfect gas relationship, the number density of molecules is given by

$$n = \frac{P}{k_B T} \tag{2}$$

where P is the pressure, T is the temperature, and k_B is the Boltzmann constant ($k_B = 1.3805 \times 10^{-23}$ J/K). At a given pressure P and temperature 273.15 K, the expression of number density is given by

$$n = 2.6544 \times 10^{20} \times P\,\mathrm{m}^{-3} \tag{3}$$

For atmospheric pressure $P = 1.013 \times 10^5$ Pa, the number density is $n \simeq 2.69 \times 10^{25}$ m^{-3}.

- *Mean molecular spacing* (δ): For uniformly spaced molecules, the mean molecular spacing is given by

$$\delta \propto n^{-1/3} \tag{4}$$

Under standard conditions, the mean molecular spacing is $\delta \simeq 3.3 \times 10^{-9}$ m. For hard sphere molecular model, the molecular diameter of air under standard conditions is given by $d \simeq 3.7 \times 10^{-10}$m. Based on the comparison of the mean molecular spacing and the mean molecular diameter, the assumption of dilute gas is valid for $\delta/d \gg 1$. Under the dilute gas assumption, binary molecular collisions are more likely than simultaneous multiple collisions.

- *Mean free path of molecules*: According to the kinetic theory of gases, the mean free path is defined as the average distance travelled by a molecule between two successive collisions. For a gas of hard sphere molecules with mean molecular diameter d, the molecular mean free path under the thermodynamic equilibrium is given by [18]

$$\lambda = \frac{1}{\sqrt{2}\pi d^2 n} \tag{5}$$

For a given pressure P, ambient temperature 300 K, and the mean molecular diameter $d = 3.7 \times 10^{-10}$m, the number density and the mean free path of air molecules are given by

$$n = 2.41 \times 10^{20} \times P\,\mathrm{m}^{-3}, \quad \lambda = \frac{0.0068}{P}\,\mathrm{m} \tag{6}$$

At ambient pressure $P = 1.013 \times 10^5$ Pa, these quantities will become $n = 2.44 \times 10^{25}$ m^{-3}, and $\lambda = 67$ nm.

- *Characteristics flow length*: It is the characteristic length of the flow channel through which the fluid flows. For some cases, it may be a characteristic dimension of the body itself or the diameter of an internal flow conduit. For other cases, it may be the boundary layer thickness, etc. For the present case, the air-gap thickness h between the oscillating plate and the fixed substrate is taken as the characteristics flow length [26].

Division of Flow Regimes

According to the degree of rarefaction, the rarified gas flow is divided into three main flow regimes, i.e., the slip flow regime, the transitional flow regime and the free molecular flow regime. Based on the values of Knudsen number, the different flow regimes are defined in Table 1 [18].

In the slip flow regime, some phenomena such as velocity slip and the temperature jump in the vicinities of the boundaries occur, which are different from those in the ordinary continuum flows. In this regime, we can still use the usual dynamic equations or equations of higher order (than Navier–Stokes) obtained using higher order terms in Chapmann–Enskog expansion [18, 27–29], but it is necessary to modify the boundary conditions.

For extremely rarified flows, the mean free path λ becomes much greater than the characteristic body dimension h of the micro mechanical structures. In this case, no boundary layer is formed and the molecules reflected from a surface do not collide with mean free stream molecules until far away from the body. Consequently, any distortion of the free stream velocity distribution, which is the equilibrium Maxwell distribution, can be neglected. In this case, the flow phenomena is mostly governed by molecule-surface interaction. This regime is called the free molecular flow regime [16, 18].

In the transitional flow regime between the slip flow regime and the free molecular regime, the mean free path is of the same order as the typical characteristic flow length. The collisions of the molecules with the surface of the body and intermolecular collisions are of more or less equal importance and consequently the analysis becomes very complicated [16, 26].

As an alternative approach, we solve 3D Navier–Stokes equation using ANSYS for pressure distribution under different flow regimes by taking effective viscosity of the fluid which captures the slip boundary condition [9, 25]. However, like other approaches based on continuum equations, this approach also fails at a certain value of Kn which will be discussed later.

Table 1 Characterization of different flow regimes

Range of Kn	Flow regime
Kn < 0.01	Continuum flow regime
0.01 < Kn < 0.1	Slip flow regime
0.1 < Kn < 10	Transition flow regime
Kn > 10	Molecular flow regime

Similarity of Microflows

For two flows, the same Knudsen number may be obtained due to different characteristic length h and different gas density (thus the mean free path). The expression for Kn, which is obtained by combining equations (1) and (5), is given by

$$\mathrm{Kn} = \frac{\lambda}{h} = \frac{0.0068\ \mathrm{N/m}}{P\,h}. \tag{7}$$

Thus, by changing P and h appropriately, one can get the same Kn in various cases. This suggests similarity of flows (as far as rarefaction is concerned) in such cases. However, this similarity law is not valid under all conditions, especially when the characteristic length scale of the problem is extremely small. This is because the real number of molecules in the characteristic volume may be so small that the problem of fluctuation in the calculation of average value of macroscopic quantities must be considered [26]. Moreover, the effect of surface roughness also becomes important in the case of extremely narrow channels. Therefore, equation (7) can be used as a scaling law under the condition that the statistical fluctuation is limited below 1%. Under this condition, the ratio of characteristic length h to the mean molecular spacing δ should be greater than 20, i.e., $h/\delta > 20$.

In the present study, we take a fixed value of the characteristic flow length and then vary the surrounding pressure P to obtain experimental quality factor under different flow regimes listed in Table 1.

Sample Preparation

Figure 1 shows the SEM image of the double-gimbaled MEMS torsional resonator. The resonator is fabricated using MUMPS poly-silicon surface micromachining process. The mirror plate, 400μm $\times$ 400μm

in area, was made out of Poly1–Traped-Oxide–Poly2 sandwich structure with a total thickness of 4.25μm. The width, thickness and length of the two pairs of torsional beams are 2μm, 1.5μm, and 180μm respectively. After fabrication, the micromirror was manually elevated under a microscope. The micromirror, torsional beams, inner and outer frames were raised up to a height of 80μm from the substrate by pushing four sliding plates simultaneously towards the mirror center until they locked using the mechanical latching structures.

Kinematics and Dimensions of the Test Structure

Figure 2 shows a schematic diagram of the MEMS torsional resonator with two sectional views along A-A′ and B-B′, respectively. In this dual axis resonator, there are two types of motion, one about the y-axis and the second about the x-axis. For the motion about the y-axis, only the inner plate vibrates with angular displacement θ as shown in Fig. 2(b). This motion is obtained by electrostatic actuation using electrodes E_1 and E_4 or E_2 and E_3 placed under the inner plate. In this case, rest of the structures, such as the inner frame, the outer torsion beams and the outer frame, are stationary. The fluid damping due to this motion is just because of the flow around the inner plate and the nearby frame, which acts as an obstacle in the flow from the outer boundary of the inner plate. In the other motion about the x-axis, the inner frame vibrates along with the inner plate and the inner torsional beams about the x-axis with an angular displacement ϕ as shown in Fig. 2(c), while the outer frame remains stationary. In this case, oscillations are caused by electrostatic actuation using electrodes E_1 and E_2 or E_4 and E_3.

The two inner torsional bars along the y-axis that act as springs for the torsional vibration θ about the y-axis, connect the inner plate to the inner frame. The two outer torsional bars, which act as springs during the torsional motion ϕ about the x-axis, connect the inner frame to the outer fixed frame. The size of the inner square plate is $l_p \times l_p \times t_p$. The inner frame has an inner hollow rectangle of size $l_{\text{if}} \times b_{\text{if}}$, and its width and the thickness are w_{if} and t_{if}, respectively. The outer frame has an outer rectangle of size $l_{\text{of}} \times b_{\text{of}}$, and its width and thickness are w_{of} and t_{of}, respectively. The inner and outer sides of the square electrode E_1, E_2, E_3, or E_4 are separated from the center of the torsional bars, along the x- or y-axes, by a distance a and b ($> a$), respectively [see Fig. 2(b) and (c)]. The air gap thickness is h. The length, width, and thickness of the inner and outer torsional bars are l_{in}, w_{in}, and t_{in}; and l_{out}, w_{out}, and t_{out}, respectively. The inner plate has $M \times M$ uniformly distributed square perforations ($M = 13$), each with side length p. The inner and outer frames also contain perforation of the same size as shown in Fig. 2. Finally, we summarize the dimensions and the material property of the mirror in Table 2.

The view A-A′ presents the angular displacement, θ, of the inner plate from its zero position. The view B-B′ shows angular displacement, ϕ, of the inner frame (with inner plate and inner springs) with respect to its zero position. The angular deflections ϕ and θ are due to the combined effects of electrostatic, elastic and fluid forces. The electrostatic force is applied such that the displacements are small so that the harmonic motion is maintained. Under the ambient condition, the flows in the air-gap (= 80 μm) and that around the moving structure are in the continuum regime because Kn> 0.001 for $h_0 = 80$ μm, $P = 1.013 \times 10^5$ Pa. The higher values of Kn are obtained by reducing the surrounding pressure P. The total fluid damping due to the fluid flow in two different motions is caused by the following factors:

- Squeeze-film damping: It is caused due to the squeezing of the fluid flow between the moving structure and the fixed substrate. It is the most significant effect among all types of fluid damping, if it exists [9, 21].
- Damping due to drag forces: It is due to the flow of air on the top of the moving structure which causes some loss of energy. This loss is generally negligible if the gap between the moving structure and the fixed substrate is small, so that the squeeze-film damping is very high. But for large gaps between the vibrating structure and the fixed substrate, the drag forces become the dominant loss mechanism for the fluid damping [30].
- Loss due to perforations: Generally, the perforations provided on the structure are used for efficient etching process. But, they also help in reducing the fluid damping. Since the size of the square perforation (3 μm ×3 μm) is very small compared to the pitch of the perforations (32.5 μm) and the air-gap thickness (80 μm), the effect of perforations on the fluid damping is negligible compared to the fluid damping in the air-gap thickness [31, 32].
- Miscellaneous factors: The presence of nearby structures, such as the stationary inner frame during the motion about the y-axis and the stationary outer frame during the motion about the x-axis, can increase the fluid damping effectively. Hence, these factors should be considered while modelling the fluid damping.

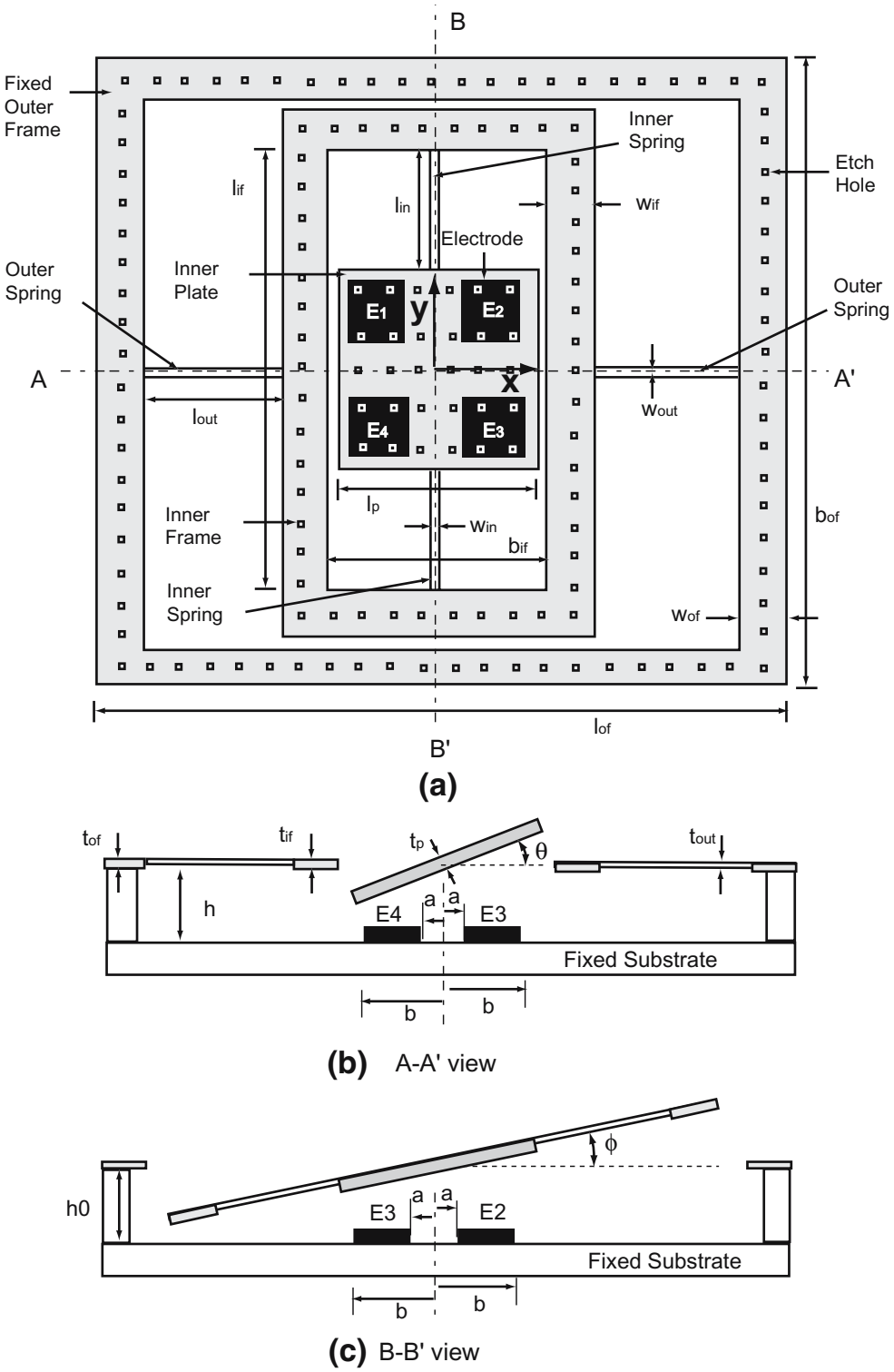

Fig. 2 Schematic diagram of the double-gimballed torsion mirror (**a**) and its sectional views along A-A′ (**b**) and B-B′ (**c**)

Experimental Studies

In this section, we first discuss the experimental set-up and the procedure to calculate the quality factor of the device for the motion about the x- and y-axes, respectively. Later, we present the experimental results and discuss the nature of variation of the quality factor with the surrounding pressure. Finally, we discuss different sources of error that must be kept in mind while performing experiments for low pressure measurements.

Table 2 Dimensions of the MEMS torsion mirror shown in Fig. 2

Symbol	Description	Values
l_p	Length of the inner plate	400 μm
b_p	Width of the inner plate	400 μm
t_p	Thickness of the inner plate	4.25 μm
l_{if}	Length of the inner frame	778 μm
b_{if}	Breadth of the inner frame	438 μm
w_{if}	Width of the inner frame	52 μm
t_{if}	Thickness of the inner frame	3.5 μm
h_w	Gap between the inner plate and the inner frame	19 μm
l_{in}	Length of the inner torsional bar	180 μm
l_{out}	Length of the outer torsional bar	180 μm
w_{in}	Width of the inner torsional bar	2 μm
w_{out}	Width of the outer torsional bar	2 μm
t_{in}	Thickness of the inner torsional bar	1.5 μm
t_{out}	Thickness of the outer torsional bar	1.5 μm
p_h	Pitch of perforation	32.5 μm
l_h	Size of a single hole	3×3 μm
h_0	Air-gap thickness	80 μm
a	Inner side of the electrode from the central axis	10 μm
b	Outer side of the electrode from the central axis	170 μm
ρ_{poly}	Density of polysilicon	2300 kg/m^3
G	Shear modulus of polysilicon	6.5 $\times 10^{10}$ Pa

Experimental Procedure

Figure 3 shows the experimental set-up which is used to characterize the double gimbaled MEMS torsional resonator at different surrounding pressures P. It consist of a vacuum chamber in which the device is fixed. The vacuum is created by the vacuum pump which is connected to the chamber through the conduit. The vacuum inside the chamber is maintained at a particular pressure by closing the pressure relief valve. The pressure in the chamber is measured using the pressure gauge which is positioned between the vacuum chamber and the vacuum pump. The electrical connections are taken out from the chamber through the air-tight connectors. The bias voltage is applied using DC source, and the AC signal is applied through the function generator. The laser from the laser source is focussed on the top surface of the oscillating structure using laser pointer. The position sensing detector (PSD), which is powered using another DC source, is used to measure the displacement based on the reflected laser beam from the oscillating structure. An

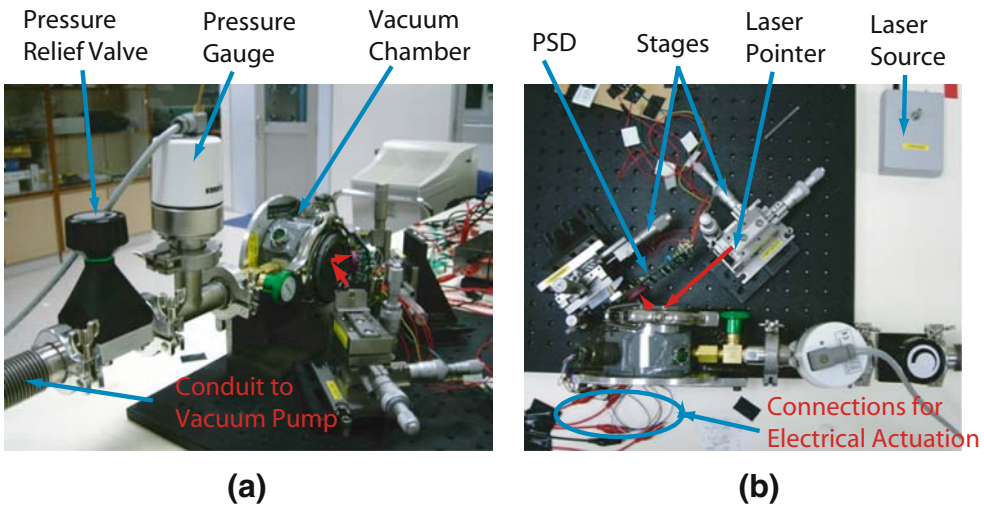

Fig. 3 Experimental set-up characterize the torsional resonator at different pressure

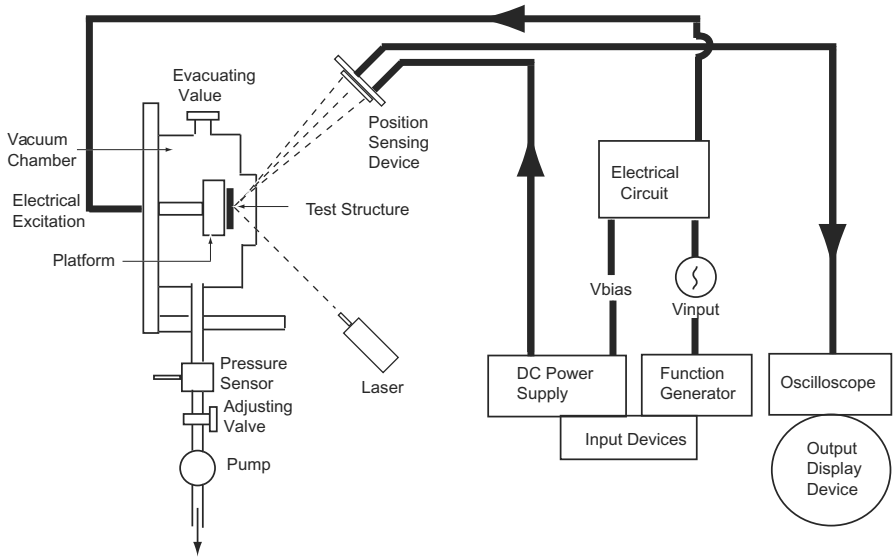

Fig. 4 Outline sketch of experimental set-up

oscilloscope is used to observe the output voltage which is related to the displacement. The working principle of the set-up is outlined in Fig. 4.

To experimentally calculate the quality factor of the double gimbaled MEMS torsion resonator at different pressures, we follow the following steps:

1. Input voltage $V = V_{\text{input}} \sin 2\pi ft$ and a bias voltage V_{bias} are applied to the electrodes. Here, f is the input frequency and t is the time. The bias voltage is varied from 20 V in the continuum regime to 3 V in the molecular regime while V_{input} is varied from 0.5 to 0.08 V. The different values of the bias voltage are used to keep the amplitude of vibration small so that the assumption of simple harmonic motion can be used to calculate damping. The maximum static displacement due to the bias voltage (20 to 3 V) is in the range of 10^{-3} to 10^{-4} rad. Therefore, any possible reduction of the air-gap thickness due to the static displacement is neglected. Due to the application of the sinusoidal voltage, an angular oscillation θ about the y-axis, and ϕ about the x-axis are obtained.
2. To measure the displacement, a laser beam is focussed at a point on the top of the vibrating plate. The laser beam reflected from the vibrating plate then falls on the PSD as shown in Figs. 3 and 4. As the plate vibrates, the voltage reading of the PSD is taken from an oscilloscope. At steady state, the voltage reading is taken which gives the angular displacement of the oscillating plate from the relation $\phi = \frac{V_p}{d}$ (in rad.). Here, V_p is the PSD output voltage (in the our experiment, the relation between the voltage and the displacement was set to 1 V $\approx$ 1 mm), and d (in mm) is the center distance between the PSD and the laser spot on the vibrating plate.
3. By collecting the displacements of both types of motion for different frequencies, we get the frequency response curve (FRF). Figure 5(a) is the FRF of the motion about the y-axis at atmospheric pressure. Similarly, the FRF under different flow regimes is obtained by reducing the surrounding pressure of the chamber from 750 to 0.001 Torr by controlling the pressure relief valve which is fixed between the vacuum chamber and the vacuum pump. Figure 5(b) shows the FRF under different flow regimes for the θ motion about the y-axis. The FRFs for low pressures are reduced and shifted because of the different values of the bias voltages. In Fig. 5(b), any frequency shift due to the change in the damping ratio from the continuum ($\xi = 0.05$) to the molecular regime ($\xi = 0.0004$) is neglected because it accounts for just 0.13%, whereas the actual frequency change is about 9%. In the same way, the FRFs of the ϕ motion about the x-axis over different flow regimes are obtained. Note that each displacement corresponding to different pressures and frequencies are repeated 10 times. Finally the average values of all the displacements are recorded.
4. Using the half-width method [33], we measure the quality factor Q_{exp} and the damping ratio ξ_{exp} from the FRF as explained in Fig. 5(a). The expression of the quality factor is given by

$$Q_{\text{exp}} \approx \frac{1}{2\xi} = \frac{f_d}{f_2 - f_1}. \tag{8}$$

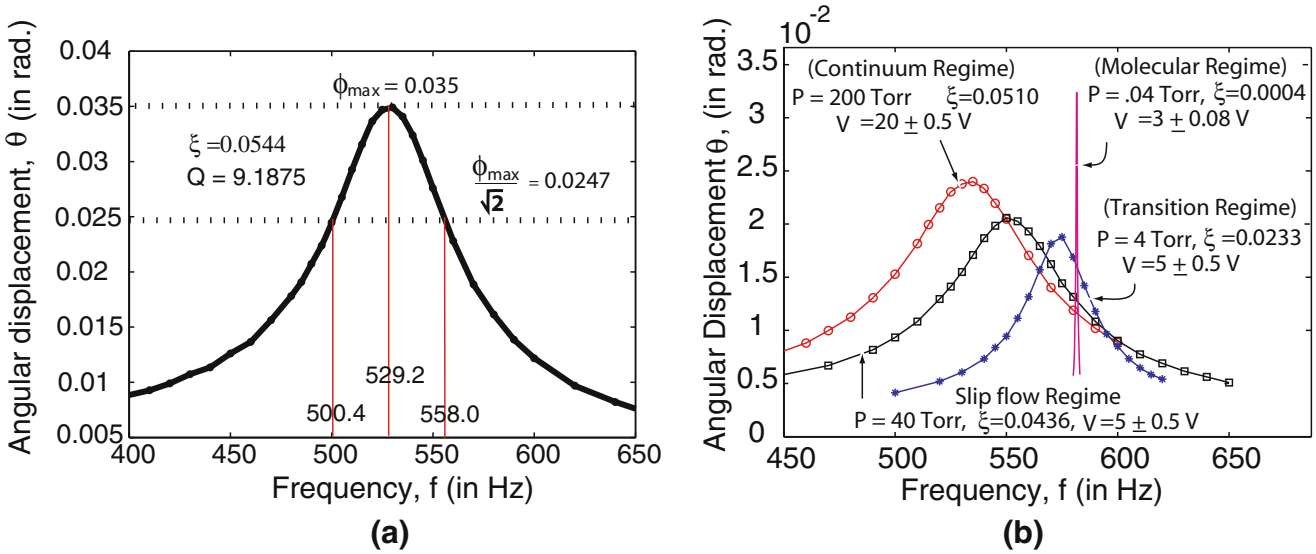

Fig. 5 FRFs for the angular motion θ at (**a**) $P = 750$ Torr; and (**b**) $P = 200, 40, 4, 0.04$ Torr

where f_d is the damped natural frequency, and f_1 and f_2 are the half power frequencies. For the case shown in Fig. 5(a), the quality factor is 9.19 ± 0.05. Similarly, the quality factor of both the motions are calculated at different surrounding pressures.

Experimental Results and Discussion

Figure 6 shows the variation of the quality factor with different values of the surrounding pressure for the torsional resonator with characteristics flow length $h = 80\ \mu$m. Based on the definition of Kn and the classification of different flow regimes discussed in "Brief Theory of Rarified Gases", the corresponding surrounding pressure P (in Torr) at $T = 300$ K is given by

$$P = \frac{0.0068}{80 \times 10^{-6}\ \text{Kn}} \times \frac{760}{1.013 \times 10^5}\ \text{Torr} = \frac{0.638}{\text{Kn}}\ \text{Torr}. \quad (9)$$

Corresponding to the values of Knudsen number over different flow regimes, the corresponding pressure ranges (in Torr) are calculated from equation (9), which give: $63.8 < P < 760$ in continuum regime, $6.38 < P < 63.8$ in slip regime, $0.0638 < P < 6.38$ in transition regime, and $P < 0.0638$ in molecular regime. By comparing the theoretical pressure range with the experimental results shown in Fig. 6, we find that the experimental results follow the theoretical regimes quite well.

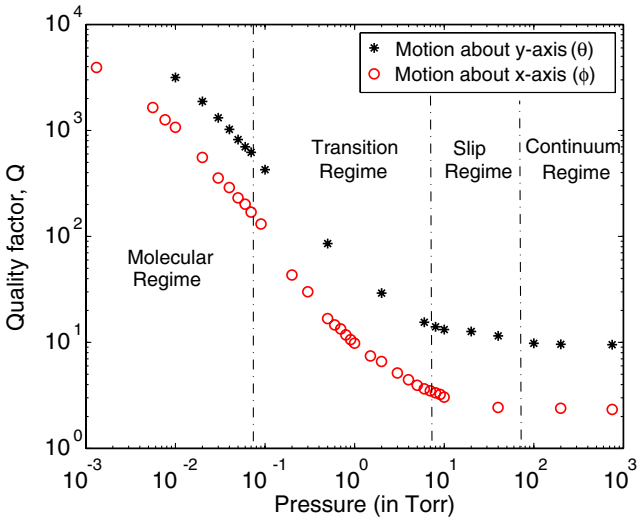

Fig. 6 Experimentally computed quality factor Vs pressure for motion about the inner torsion bar (θ) and the outer torsion bar (ϕ)

Now, if we compare the quality factors of two different motions, θ and ϕ, we find that the quality factor of the motion about the y-axis (θ) is an order of magnitude higher than that of the motion about the x-axis (ϕ). The lower value of the quality factor of ϕ motion is because of the additional damping obtained from the oscillation of the inner frame. The fluid damping in θ motion is due to the squeeze-film damping between the inner plate and the fixed substrate, and the drag force due to the air-flow on the top of the inner plate. But in the case of ϕ motion, in addition to the damping present in the θ motion, additional squeeze-film damping and loss due to drag forces are added due to the motion of the inner frame as shown in Fig. 2.

When the quality factors of the two different motions are compared, it is found that $Q = 9.19$ and 2.32 for the motion about the y- and x-axes, respectively, if the fluid is in the continuum regime [see Fig. 7(a)]. If the fluid is in the slip or in the beginning of the transition regime,

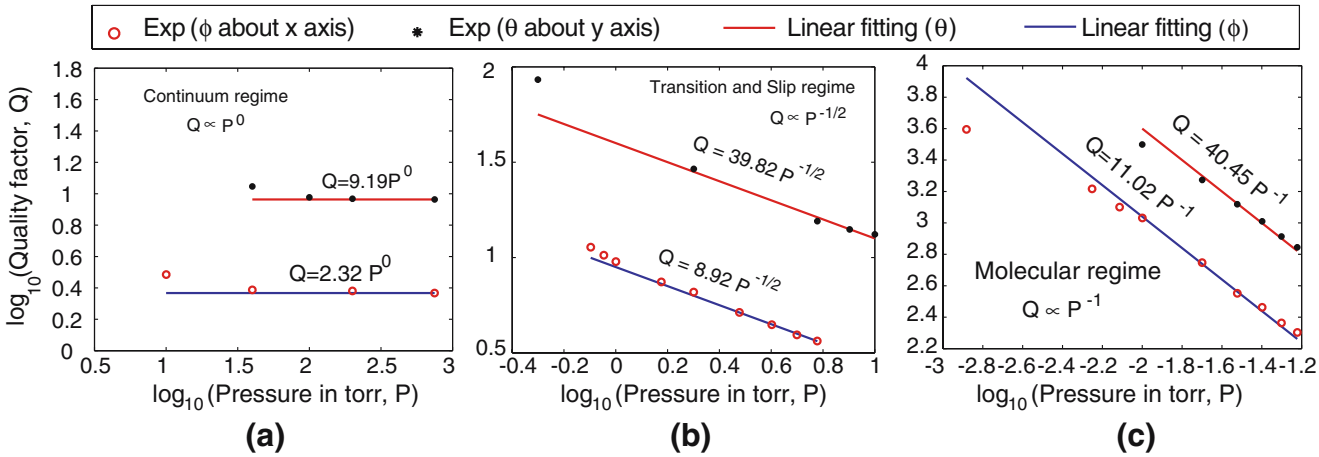

Fig. 7 Fitting of power laws over (**a**) the continuum regime, (**b**) the slip and the transition regime, and (**c**) the transition and the molecular regime

$Q = 39.82\ P^{-1/2}$ and $8.92\ P^{-1/2}$ for the θ and ϕ motions, respectively [see Fig. 7(b)]. Further, for the flow in the molecular regime, $Q = 40.45\ P^{-1}$ and $Q = 11.02\ P^{-1}$ for the motion about the x- and y-axes, respectively [see Fig. 7(c)]. From these relationships, two important points are observed. First, for a given pressure in any of the four flow regimes, the ratio of the quality factor in the motion about the y-axis and that about the x-axis is approximately constant, and is equal to 4. However, this ratio falls down after the molecular regime where the fluid damping ceases. It is also observed that as this ratio decreases in the molecular regime, the quality factor of the motion about the y-axis remains noticeably higher compared to that about the x-axis because of comparatively large peripheral length and small resonance frequency [10]. The above discussion reveals that the quality factor follows a particular relationship with pressure which is independent of the type of the motion but depends on the flow regime. It is also found that the quality factor seems to follow a power law $Q \propto P^{-r}$ which governs the variation of quality factor with the surrounding pressure over the entire flow regimes as shown in Fig. 8. The Q vs P variation from Figs. 7 and 8 shows that the exponent r is approximately 0 in the continuum flow regime, $\frac{1}{2}$ over the slip and a portion of the transition regime, 1 over the other portion of the transition regime and the molecular regime. On the other hand the constant of proportionality depends on the type of motion and the devices under consideration. For example, in the two different motions of the same device, we get the same Q vs P as shown in Fig. 7 but different constants of proportionality.

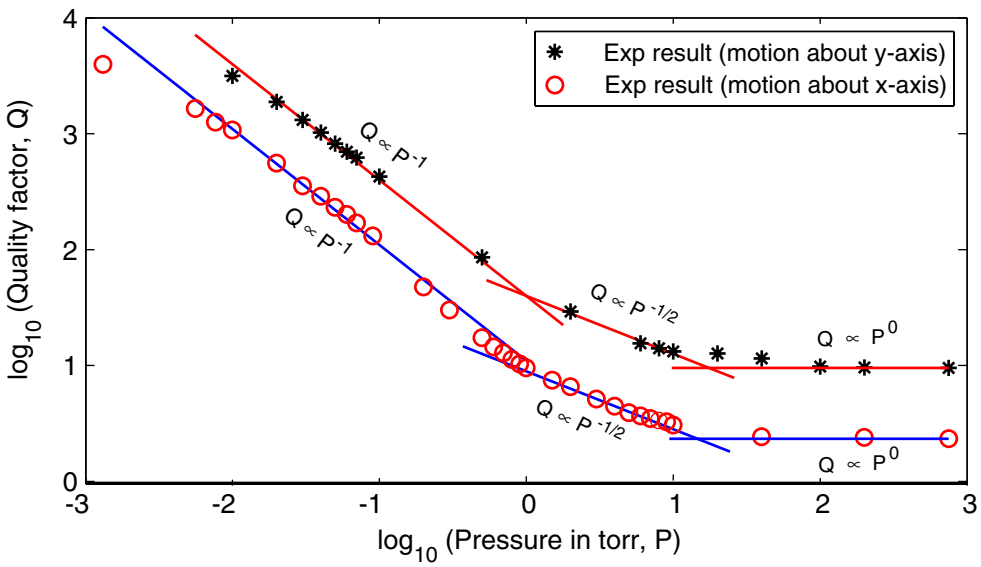

Fig. 8 Comparison between the quality factor from the experiments and that from of power laws for different flow regimes

Different Sources of Error

There are mainly fives types of error that may affect the measurement:

- *Error in pressure measurement*: This type of error is due to the difficulty in maintaining a steady state pressure condition in the vacuum chamber. The main factor against maintaining the steady state is the leakage through the clearance of the vacuum chamber. The amount of leakage which may not affect the pressure condition in the continuum and slip regimes, may become a significant source of error when the pressure in the chamber is reduced to high vacuum. This type of error can be minimized by using a more stringent air-tight vacuum chamber. In the present case, pressure measurement is taken after observing the steady state condition. The duration of steady state condition varies for the flow in the continuum regime to the flow in the molecular regime.
- *Error due to the input voltage*: After maintaining the steady-state of the operating condition in the chamber, the voltage is applied to excite the structure. It is observed that the oscillating structure becomes unstable if the same bias voltage is maintained for actuating the structure under all the flow regimes. Therefore, smaller values of bias and AC voltages are selected to avoid this condition. Thus, the different excitation forces, which are used in the measurements of FRF of the oscillating structure, in different flow regimes can lead to some amount of error in the measurement of the quality factor. This error is minimized by using the minimum value of the bias voltage. In the present case, to avoid the instability of the device and keeping the error due to a large bias voltage to a minimum, the bias voltage is varied from 20 V for the flow under the continuum regime to 3 V for that under the molecular regime. The different values of the bias voltage shift the resonant frequency as shown in Fig. 5(b). The AC voltage should be very small compared to the bias voltage.
- *Error due to the PSD measurement*: The output from the PSD is obtained from the movement of the oscillating laser spot on the sensing area of the PSD. The sensing area of the PSD has limitations in terms of displacement measurements. If the laser spot crosses the sensing area, then the output voltage will be in the form of a chopped signal. To avoid such condition, the distance between the PSD and the vacuum chamber has to be kept as small as possible.

  Another factor that can lead to wrong values in the measurement is the position of the laser spot on the test structure. Although it is obvious, the laser spot should be carefully directed on the moving part of the structure otherwise the PSD will give a constant signal or a signal of very small amplitude which could be interpreted as the response of a static structure.
- *Error in reading the output signal*: The output signal from the PSD is taken through the oscilloscope. There are always some fluctuations in the amplitude of the output signal even after the steady state is reached. So, before taking the final measurement, the fluctuation about the fixed value of the output signal is observed carefully. After the fluctuations become constant, ten readings of the amplitude of the output signal are taken at different times. Finally, the average of the ten readings is taken as the final output data. These steps are repeated for taking the output data for each frequency under different surrounding pressures.
- *Error in quality factor measurement*: This type of error depends largely on the smoothness of the FRF around the peak. To minimize the error in calculating the quality factor using the half-width method, the measurements are taken at sufficient number of frequencies to get a smooth FRF, especially at and around the peak where the peak reduces to its $1/\sqrt{2}$ value.

Repeatability and precision

The repeatability and the precision of the experimental data can be increased by reducing the above mentioned errors. To ensure the repeatability and the precision of the experimental results, the measurements of the FRF at different pressures are repeated 10 times. The experimental results presented in the paper are the average values of the 10 independent readings. The standard deviation of the measurements of quality factor over the pressure range of 750 to 0.001 Torr are found to be in the range of 0.03 to 0.08 for the angular motion θ and 0.04 to 0.1 for the angular motion ϕ. From the values of the standard deviation for both the motions, it is found that the experimental results have good repeatability and precision.

Comparison with Numerical Simulation

To consider rarefaction effect, the pressure distribution can be found either by solving the Boltzmann equation using DSMC method [22] or by solving the

Navier–Stokes equation with slip boundary conditions [16]. The first approach which is based on the statistical method is generic, while the second approach which is based on the continuum theory with certain modifications, is limited by the degree of rarefaction. It is found that for small air-gap to length ratio the Navier–Stokes equation is reduced to the Reynolds equation. Under the assumption of incompressible, inertialess and isothermal flow conditions, the rarefaction effect can be captured by modifying the dynamic viscosity of the fluid [9]. The effective viscosity for the poiseuille flow under different flow regimes corresponding to a higher-order velocity slip boundary condition is given by [9, 25]

$$\mu_{\text{eff}} = \frac{\mu}{1 + 3\sqrt{\pi}.a.D^{-1} + 6b.D^{c}} \tag{10}$$

where μ is dynamic viscosity, $D(=\sqrt{\pi}/2\text{Kn})$ is the inverse Knudsen number to capture rarefaction effect, Kn is the Knudsen number, $a = 0.01807$, $b = 1.35355$ and $c = -1.17468$. In this paper, we use the second approach to calculate pressure distribution. The numerical procedure and its validation are described through a simple verification problem in the next section.

Verification Problem

To verify the concept of using effective viscosity for considering the rarefaction effect in the numerical simulation, we consider a 2D flow problem as shown in Fig. 9(a). In this case, the structure of length L_x which is separated from the fixed substrate by h_0 executes torsional motion. The squeeze-film damping due to the flow through the air-gap can be determined by solving the 1-D Reynolds equation with zero pressure boundary conditions. For the air of density ρ and the absolute viscosity μ, the quality factor based on the squeeze-film damping torque can be determined from [8]

$$Q_{\text{anal}} = \frac{60 I\omega h_0^3}{\mu_{\text{eff}} L_x^5} \tag{11}$$

To numerically calculate the quality factor due to fluid damping in the test structure shown in Fig. 1, the 2-D domain shown in Fig. 9(a) is meshed with FLUID141 element in ANSYS. Then the Navier–Stokes equation is solved under the boundary conditions shown in Fig. 9(a) to get the pressure distribution. The zero pressure boundary condition is applied on the sides, the zero velocity boundary condition is applied on the bottom and the $\theta = \theta_0 \sin \omega t$ is applied on the top line about the mid-point. Here, no-slip condition is used but the effective viscosity is taken to capture the effect of slip on the boundaries under the rarified flow regimes. From the back pressure distribution, the damping torque $T_d = T_{\max} \cos \omega t$ is determined by integrating the moment of the back force about the axis of oscillation. Finally, the numerically computed quality factor is determined from the following equation [33]:

$$Q_{\text{num}} = \frac{I\theta_0\omega^2}{T_{\max}} \tag{12}$$

To validate the numerical procedure, we compare the numerically computed quality factor with the analytical value obtained from equation (11) for $L = 100\ \mu$m, and $h_0 = 1\ \mu$m. The air is used as the surrounding medium. The density and the absolute viscosity of air are taken

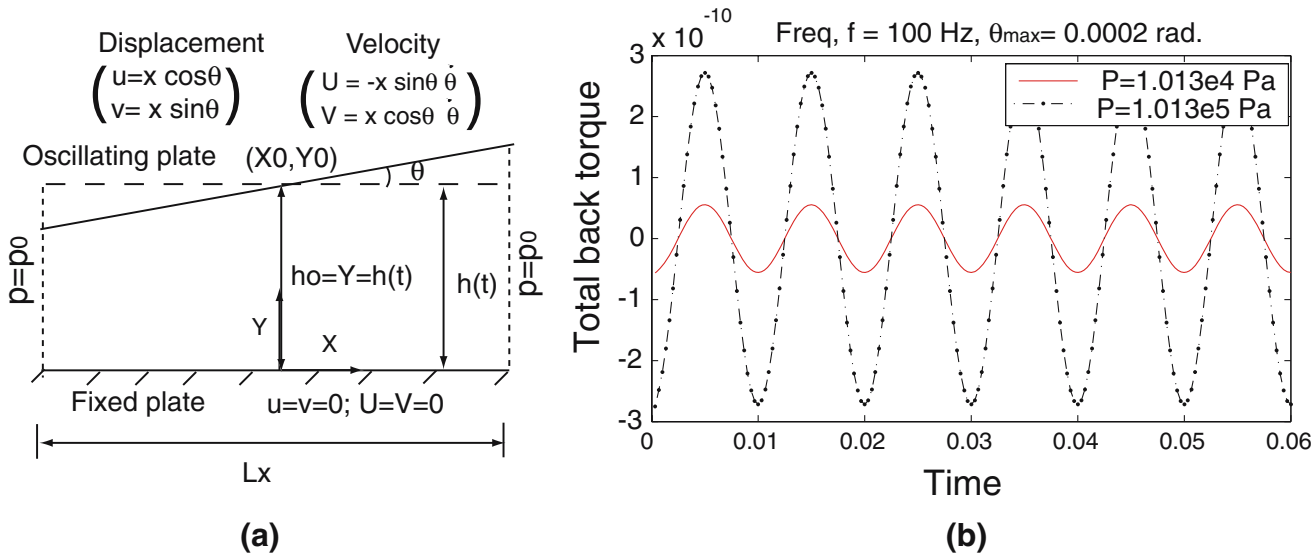

Fig. 9 (**a**) 2D fluid domain for determining the pressure distribution due to 1-D torsional motion. (**b**) Transient response of the total back torque

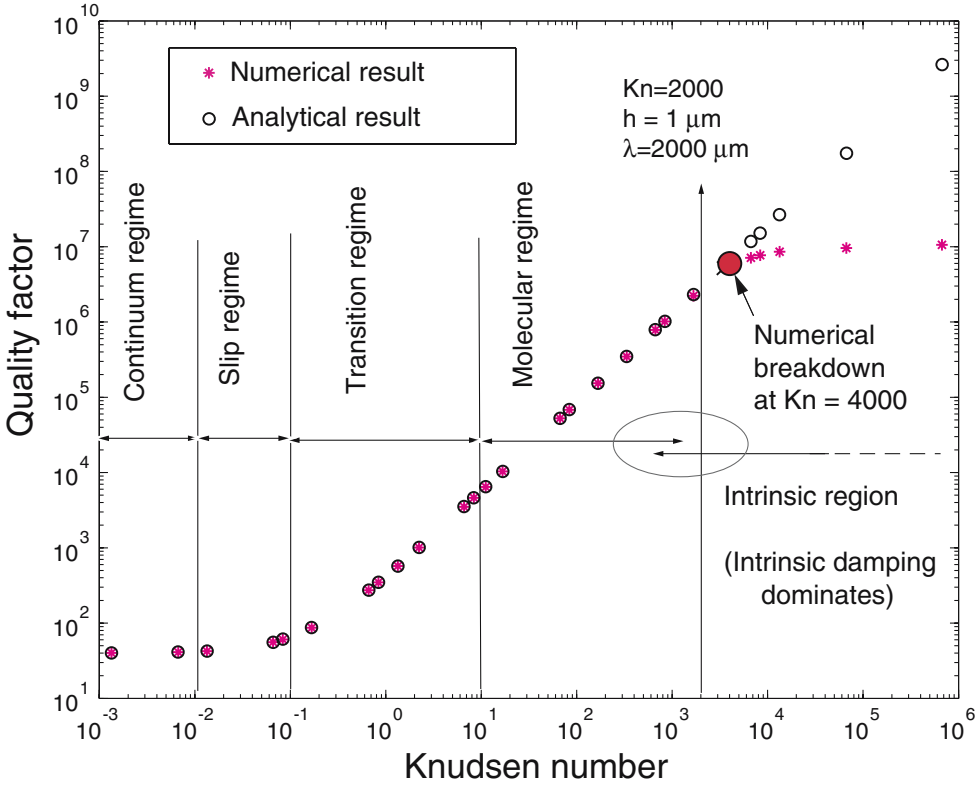

Fig. 10 Comparison between the analytically and the numerically calculated quality factor with respect to Kn for 1-D torsional motion

to be 1.2 kg/m^3 and 1.8×10^{-5} N-s/m^2, respectively. While the excitation frequency is 100 Hz, the amplitude of angular displacement θ_0 is taken as 0.0002 rad corresponding to 1% of the maximum allowable angular displacement when the tip of the structure touches the substrate.

Figure 9(b) shows the damping torques corresponding to the surrounding pressure P of 750 and 75 Torr. Figure 10 shows the comparison of the numerical and the analytical results under different flow regimes ($0 <$ Kn $< 10^6$). The higher limit of Kn is impractical as the quality factor ($> 10^5$) under this regime is generally dominated by the intrinsic or other pressure independent losses [34]. Here, the higher range of Kn is selected to find the limitation of the numerical procedure. It is found that both the results match very well till Kn $= 4000$. Thereafter, the numerical results give erroneous values. After doing similar numerical experiments for higher values of the characteristic flow length h_0 and constant value of L_x, it is found that the numerical procedure fails at decreasing values of Kn. Thus, it is noted that the failure point depends on the ratio of h_0/L_x. The numerical procedure as explained above can be used as an alternate tool to consider rarefaction effect over almost all flow regimes with an error of less than 10% if $h_0/L_x < 0.1$. Even this error become less than 1% if $h_0/L_x < 0.01$. In the subsequent section, we compare the numerical results with the experimental results for even higher value of h_0/L_x(=0.2).

Comparison of Numerical and Experimental Results

To numerically find the quality factor due to the fluid damping, we create a 3-D fluid domain around the torsional resonator of the given dimensions (see Table 2). Let us first model the fluid flow due to the angular motion θ about the y-axis. The cross-section of the 3-D fluid domain is shown in Fig. 11. The side boundaries

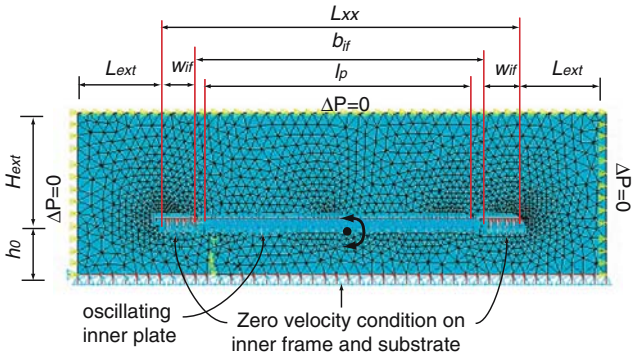

Fig. 11 Cross-section of the 3-D fluid domain around the oscillating structure for the angular motion θ as shown in Fig. 2(b)

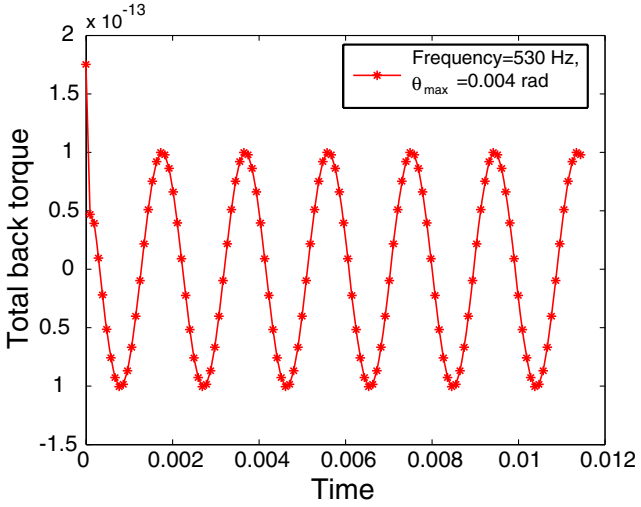

Fig. 12 Transient response of total back torque for the angular motion θ

are extended by L_{ext} and the top boundary by H_{ext}. The value of L_{ext} and H_{ext} are obtained by gradually moving the boundary outwards until the obtained solution converges for the pressure distribution around the structure. The fluid domain is meshed with tetrahedral FLUID 142 elements of ANSYS. The zero pressure boundary condition is applied on the extended surfaces; zero velocity condition is applied on the bottom surface and the surfaces around the static frame; and the sinusoidal angular velocity $\dot{\theta} = \theta_0 \omega \cos \omega t$ is applied on the surfaces binding the moving structure.

To find the transient response, the simulation is done for six cycles because six cycles are found to be sufficient to attain the steady state as shown in Fig. 12. On the time axis, 20 points are used per cycle. At each time step, local iterations are done to achieve convergence of order five in the calculation of pressure variation. After calculating the total reactive torque, we calculate the quality factor from equation (12). The numerical error is found to be below 1% if the number of tetrahedral FLUID 141 is taken over 250,000. The converged values of the maximum torque T_{max} is found to be 1.03×10^{-13} N-m (for about 4×10^5 tetrahedral FLUID 141 elements) corresponding to the angular oscillation $\phi = 0.004 \sin(3325.10\, t)$. Finally, the quality factor under the operating pressure of $P = 750$ Torr is found to be $Q_{num} = 9.27$ which is very close to the experimentally determined quality factor $Q_{exp} = 9.19$. The percentage error is found to be less than 1%. Similarly, the quality factor at different pressures are calculated. Figure 13(a) shows the comparison between the numerical and the experimental values of the quality factor for the angular motion θ. The same procedure is repeated for the angular motion ϕ. For this motion, the numerically computed quality factors are compared with the experimental values in Fig. 13(b). The percentage error in this case is found to be about 9% at $P = 750$ Torr. The large error in this case is because of insufficient extension of the domain boundaries in which the effect of outer static frame is also considered. The inability to further extending the outer boundaries is limited by the maximum number of nodes permissible in ANSYS.

By comparing the numerical and the experimental results, it is found that the numerical results give erroneous values after Kn = 6.3. It is also noted that

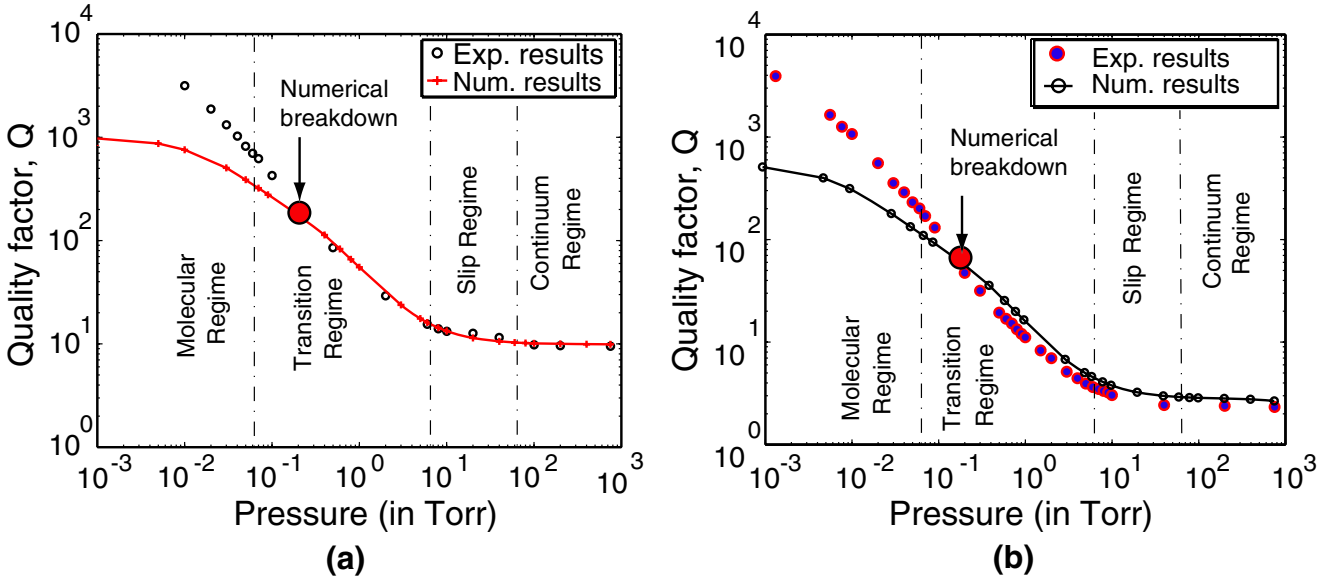

Fig. 13 Comparison between experimental and numerical results for the torsional motion about (**a**) the inner torsion bar (θ) and (**b**) the outer torsion bar (ϕ) of the torsional resonator shown in Fig. 1

the numerical results follow the same pattern as the experimental results for the motion about both the axes till Kn= 6.3. This also provides a check on the precision of the experimental results presented in this paper.

Conclusions

Effect of surrounding pressure on the quality factor of a MEMS torsion resonator is studied experimentally and numerically. The variation of the experimental quality factor Q with the surrounding pressure P explicitly shows the division of the entire curve into four different flow regimes. The theoretical prediction in different flow regimes is followed well by the experimental results. The experimental quality factor Q follows a power law $Q \propto P^{-r}$, where $r \approx 0$ in the continuum regime, $r \approx \frac{1}{2}$ in the slip regime and $r \approx 1$ in the free molecular regime. To numerically model the rarefaction effect in different flow regimes for the torsional resonator, we solve the Navier–Stokes equation with appropriate boundary conditions. In this paper, we use the concept of effective viscosity to consider the corresponding slip boundary condition. After verifying the procedure with the analytical result for a simple case, we find that using the effective viscosity model is equivalent to considering the slip boundary condition. However, the shortcoming of this method is that it fails after a particular value of Kn. The failure point depends on the ratio of the air-gap thickness to the lateral dimensions of the oscillating structure. It is also found that the failure point lies much beyond the molecular regime for $h_0/L < 0.01$, while it occurs somewhere in the transition regime (Kn= 6.3) for the present device in which $h_0/L = 0.2$. Finally, we remark that the experimental results presented in this paper have good repeatability and precision. The numerical method which is proposed to consider the rarefaction effect can be used effectively for small air-gap to lateral length ratios ($h_0/L < 0.01$) even in the molecular regime.

Acknowledgements This work is partially supported by a grant from the Department of Science and Technology, Government of India and the National University of Singapore, Singapore.

References

1. Craighead HG (2000) Nanoelectromechanical systems. Science 290(5496):1532–1535.
2. Ilic B, Yang Y, Craighead HG (2004) Virus detection using naoelectromechanical devices. Appl Phys Lett 85(1313): 2604–2606.
3. Verbridge SS, Parpia JM, Reichenbach RB, Bellan LM, Craighead HG (2006) High quality factor resonance at room temperature with nanostrings under high tensile stress. J Appl Phys 99:124304–124308.
4. Blom FR, Bouwstra S, Elwenspoek M, Fluitman JHJ (1992) Dependence of the quality factor of micromachined silicon beam resonators on pressure and geometry. J Vac Sci Tech B 10(1):19–26.
5. Langlois WE (1962) Isothermal squeeze films. Q Appl Math 20(2):131–150.
6. Griffin WS, Richardsen HH, Yamamami S (1966) A study of fluid squeeze film damping. J Basic Eng 88:451–456.
7. Blech JJ (1983) On isothermal squeeze films. J Lubr Technol 105:615–620.
8. Pan F, Kubby J, Peeters E, Tran AT, Mukherjee S (1998) Squeeze film damping effect on the dynamic response of a MEMS torsion mirror. J Micromechanics Microengineering 8:200–208.
9. Chang K-M, Lee S-C, Li S-H (1999) Squeeze film damping effect on a MEMS torsion mirror. J Micromechanics Microengineering 9(1):89–96.
10. Minikes A, Bucher I, Avivi G (2005) Damping of a microresonator torsion mirror in rarefied gas ambient. J Micromechanics Microengineering 15:1762–1769.
11. Huang JM, Liu AQ, Deng ZL, Zhang QX, Ahn J, Asundi A (2004) An approach to the coupling effect between torsion and bending for electrostatic torsional micromirrors. Sens Actuators A Phys 115:159–167.
12. Zhou G, Tay FEH, Chau FS (2003) Macro-modelling of a double-gimbaled electrostatic torsional micromirror. J Micromechanics Microengineering 13:532–547.
13. Arkilic EB, Breuer KS (1993) Gaseous flow in small channels. AIAA Pap 93:3270-1–7.
14. Arkilic EB, Breuer KS, Schmidt MA (2001) Mass flow and tangential momentum accommodation in silicon micromachined channels. J Fluid Mech 437:29–43.
15. Colin S (2005) Rarefaction and compressibility effects on steady and transient gas flows in microchannels. Microfluid Nanofluid 1:268–279.
16. Kogan MN (1969) Rarified gas dynamics. Plenum, New York.
17. Sharipov F (1999) Non-isothermal gas flow through rectangular microchannels. J Micromechanics Microengineering 9:394–401.
18. Bird GA (1996) Molecular gas dynamics and the direct simulation of gas flows. Oxford University Press, Oxford.
19. Beskok A, Karniadakis GE (1999) A model for flows in channels, pipes, and ducts at micro and nano scales. Microscale Thermophys Eng 3(1):43–77.
20. Batchelor GK (1997) An introduction to fluid dynamics. Cambridge University Press, Cambridge.
21. Pan LS, Liu GR, Lam KY (1999) Determination of slip coefficient for rarefied gas flows using direct simulation Monte Carlo. J Micromechanics Microengineering 9(1):89–96.
22. Piekos ES, Breuer KS (1996) Numerical modeling of micromechanical devices using the direct simulation Monte Carlo method. J Fluids Eng 118:464–469.
23. Sharipov F, Seleznev V (1998) Data on internal rarefied gas flows. J Phys Chem Ref Data 27(3):657–706.
24. Cercignani C (1998) The boltzmann equation and its application. Springer, New York.
25. Li W-L (1999) Analytical modeling of ultra-thin gas squeeze film. Nanotechnology 10(4):440–446.
26. Karniadakis GE, Beskok A (2001) Micro flows: fundamental and simulation. Springer, New York.
27. Bhatnagar P, Gross K, Krook K (1954) A model for collision processes in gasses. Phys Rev 94:511–524.
28. Cercignani C, Illner R, Pulvirenti M (1994) The mathematical theory of dilute gases, vol. 106. Springer, New York.

29. Grad H (1949) On the kinetic theory of rarefied gases. Commun Pure Appl Math 2:331–407.
30. Veijola T, Pursula A, Råback P (2005) Extending the validity of squeezed-film damper models with elongations of surface dimensions. J Micromechanics Microengineering 15:1624–1636.
31. Pandey AK, Pratap R, Chau FS (2007) Analytical solution of modified Reynolds equation in perforated MEMS structures. Sens Actuators A Phys 135:839–848.
32. Pandey AK, Pratap R (2007) A comparative study of analytical squeeze film damping models in rigid rectangular perforated MEMS structures with experimental results. Microfluid Nanofluid, doi:10.1007/s10404-007-0165-4.
33. Rao SS (1995) Mechanical vibration. Wesley, New York.
34. Mohanty P, Harrington DA, Ekinci KL, Yang YT, Murphy MJ, Roukes ML (2002) Intrinsic dissipation in high-frequency micromechanical resonators. Phys Rev B 66:085416-1–15.